Planetary Boundary Layer Heights from Cruises in Spring to Autumn Chukchi-Beaufort Sea Compared with ERA5

Mingyi Gu[1], G. W. K. Moore[2*], Kevin Wood[3], Zhaomin Wang[4,5*]

[1]School of Atmospheric Sciences, Nanjing University of Information Science and Technology, Nanjing, China

[2]Department of Physics, University of Toronto, Ontario, Canada

3Joint Institute for the Study of the Atmosphere and Ocean (JISAO), and

NOAA Pacific Marine Environmental Laboratory, University of Washington, Seattle, Washington, USA

[4]College of Oceanography, Hohai University, Nanjing, China

[5]Southern Marine Science and Engineering Guangdong Laboratory (Zhuhai), Zhuhai, China

*Corresponding author: G. W. K. Moore (gwk.moore@utoronto.ca), Zhaomin Wang (zhaomin.wang@hhu.edu.cn)

Key Points:

- Planetary boundary layer heights (PBLH) from five icebreaker cruises in the Chukchi and Beaufort Seas were examined and compared with ERA5
- Clear seasonal changes were found in both observed and reanalysis PBLH.
- The biases in the ERA5 PBLH were found to be a function of wind direction with larger biases occurring for northerly flow situations.

Abstract

The planetary boundary layer height (PBLH) is a diagnostic field related to the effective heat capacity of the lower atmosphere and it constrains motion in this layer as well as impacting surface warming. Here we used radiosonde data from five icebreaker cruises to the Chukchi and Beaufort Seas during both spring and fall to derive PBLH that were compared with results from the ERA5 reanalysis. The ERA5 PBLH was similar to but slightly lower than the observation. Clear and consistent seasonal changes were found in both the observation and the reanalysis: PBLH decreases from mid-May to mid-June and subsequently increases after August. The comparison with ERA5 shows that biases in PBLH are a function of wind direction that are largest for northerly flow conditions, suggesting that the availability of upwind observations is important in representing processes active in the planetary boundary layer over the Arctic Ocean.

Plain Language Summary

In recent decades, the Arctic has been warming more rapidly than the global average. This so-called Arctic Amplification may be partly explained by the shallow boundary layer that typically occur in the Arctic thereby acting to concentrate any heating near the surface. Current climate and weather prediction models have not able to represent this characteristic of the Arctic atmosphere because of the lack of observation as well as a poor understanding of the processes active in this layer. The newly released data from a number of ice breaker cruises to the western provides an opportunity to study the Arctic boundary layer. We find that the ability of a current weather prediction model to represent the observed structure of the Arctic boundary layer is a function of wind direction suggesting a gap in our knowledge of processes that are active in this region.

1 Introduction

The Arctic has experienced a rapid warming since the 1980s, so-called Arctic Amplification (Graversen et al., 2008; Johannessen et al., 2004; Serreze et al., 2009; Serreze & Francis, 2006), and the rate of surface warming is almost twice that of the entire globe (Screen, 2014; Serreze & Barry, 2011). The planetary boundary layer (PBL) plays an important role in air-surface interactions and impacts the rate of surface warming. In addition to the retreat of sea ice (Screen & Simmonds, 2010), increased water vapor (Ghatak & Miller, 2013), the increased poleward energy transport (Yang et al., 2010), and the lapse-rate feedback (Pithan & Mauritsen, 2014), the Arctic surface warming has also been attributed to the typically shallow boundary layer in the Arctic. This is because a shallow boundary layer acts to amplify any surface warming (Bintanja et al., 2011; Esau et al., 2012; Esau & Zilitinkevich, 2010).

The PBL height (PBLH) has been recognized as an important parameter in quantifying the role of boundary layer processes in surface processes. PBLH is closely related to the effective heat capacity of the atmosphere (Esau & Zilitinkevich, 2010) and is a primary determinant of cloud type and coverage that impacts the Earth's radiation budget (Wood, 2012). PBLH varies under different climate forcing, therefore it is critical to gain an understanding of the spatiotemporal variability of the PBLH, especially in the Arctic (Davy et al., 2017; Davy & Ezau, 2014). It remains a challenge to parameterize the physical and chemical PBL processes in the climate models as these models do not resolve the shallow boundary layer and as a result, the dynamical processes in the boundary layer are often poorly simulated (Holtslag et al., 2013). There is evidence that the PBLH in both numerical weather prediction and climate models are

generally higher than the observations, especially in the cases of stable conditions (Holtslag et al., 2013; Seidel et al., 2012). Over the central Arctic Ocean during the winter, the absence of solar radiation allows the formation of a persistent stable boundary layer during cloud-free periods, while low-level clouds tend to force a shallow but relatively well-mixed boundary layer and during summer the boundary layer usually has near-neutral stability (Persson et al., 2002; Shupe et al., 2013; Tjernström & Graversen, 2009). This unique characteristic makes it important to study the Arctic PBL and its role in Arctic Amplification.

The recent studies on Arctic PBL were mainly focusing on the interaction between the PBL and clouds (Brooks et al., 2017; Lai et al., 2020; Li et al., 2020) and the sea ice (Bian et al., 2016). However, PBLH is poorly quantified, despite that limited studies have attempted to derive the PBLH using climatological mean state (Esau & Sorokina, 2011) and using the aircraft and GPS soundings observation (Dai et al., 2011).

The Arctic is a remote, sparsely populated region with very limited infrastructure (Esau & Zilitinkevich, 2010) to observe atmospheric processes. As a result, there are very limited data as to the structure and evolution of the PBL over the Arctic Ocean. The Surface Heat Budget of the Arctic Ocean experiment (SHEBA), which was conducted with a drifting icebreakers over multiyear ice in the Beaufort Sea 1997- 1998 (Persson et al., 2002), has contributed to knowledge on the surface processes in the Arctic including: examining different regimes of the stable boundary layer (Grachev et al., 2005), exploring the PBLH calculation method (Y. Zhang et al., 2014) as well as characterizing the diurnal cycle in PBLH (Liu & Liang, 2010). Some other data like "North Pole" drifting ice stations (Romanov et al., 2000), the Arctic Ocean Climate System Research observed on R/V Mirai (Inoue & Hori, 2011; Sato et al., 2012), the ASCOS measurement campaign observed on the Swedish icebreaker Oden in the summer of 2008 (Hines & Bromwich, 2017; Shupe et al., 2013) have been helpful in studying boundary layer process (Seo & Yang, 2013). However, the lack of observations in the region have limited our ability to understand the processes that determine the height of the planetary boundary layer. Here we help address this gap by using the recently released Chukchi-Beaufort icebreaker cruises radiosonde data to study Arctic PBLH, and use a new reanalysis dataset, ERA5, to examine the processes in the Arctic PBL.

2 Data and Methods

In this paper, radiosonde data from five icebreaker cruises to the Chukchi and Beaufort Seas were used to determine the evolution of the PBLH and to compare the results with those from the ERA5 reanalysis. In total, 373 individual radiosonde ascents (39 ascents from 6th August to 31st August in Louis2013; 76 ascents from 17th May to 20th June in Healy2014; 183 ascents from 5th September to 28th September in Mirai2014; 38 ascents from 26th September to 15th October in Louis2014; and 37 ascents from 24th September to 12th October in Louis2015, see Table S1-5 for details) were used in this work. The locations of the observations were shown in Figure 1. Data is available from both the late spring (May- June) as well as the early fall (August through October).

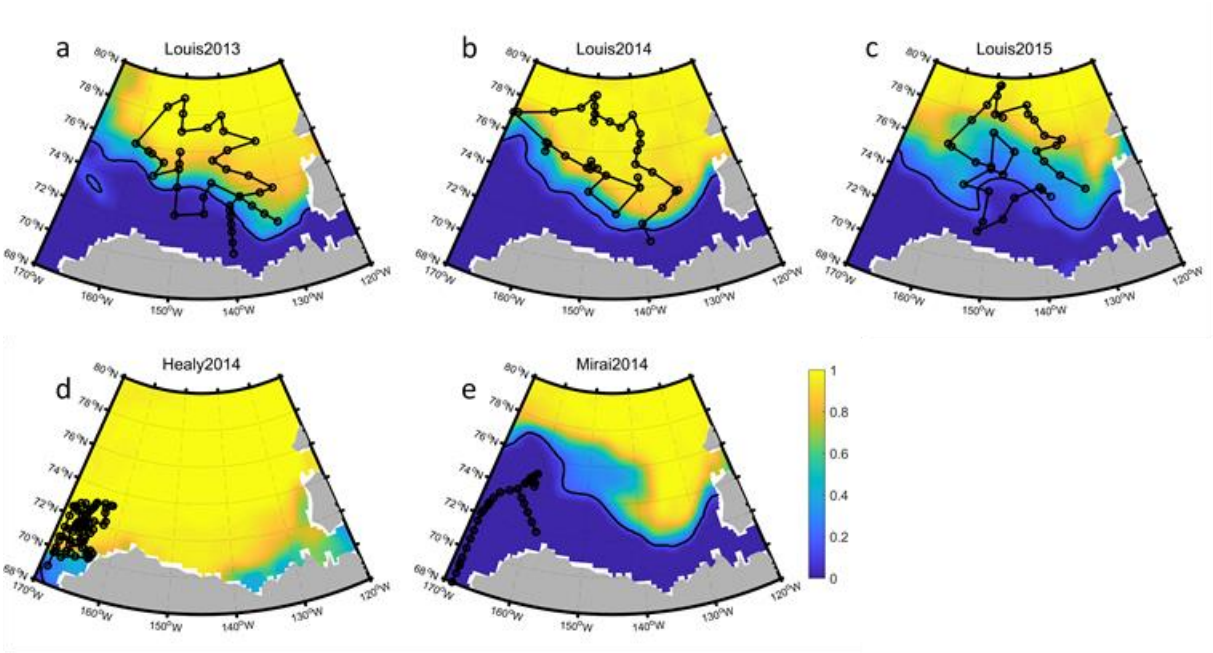

Figure 1. Cruises routes and mean sea ice concentration during Louis2013 (**a**, from 6th August to 31st August), Louis2014 (**b**, from 26th September to 15th October), Louis2015 (**c**, from 24th September to 12th October), Healy2014 (**d**, from 17th May to 20th June) and Mirai2014 (**e**, from 5th September to 28th September). Each circle with line linking shows the location of each observation along the cruise. The base colors in shading show the mean ERA5 sea ice concentration during each cruise, while the black solid line represents the 15% sea ice concentration isogram.

We use the radiosonde data to diagnose the "observed" PBLH. Seidel et al. (2012) tested several methods and found out that the bulk Ri method is the most suitable for diagnosing PBLH, as it is suitable for both stable and convective boundary layers and is not strongly dependent on vertical resolution. Following Seidel et al. (2012), the observed PBLH is found by searching upwards from the lowest observation with the PBLH defined as that level where the Ri equals the critical value of 0.25. The Ri at level k is calculated by:

$$Ri = z_k \frac{2g(s_{vk} - s_{vs})}{[(U_k - U_s)^2 + (V_k - V_s)^2](s_{vk} + s_{vs} - gz_k - gz_s)},$$

$$where\ s_{vk} = c_p T_k(1 + \varepsilon q_k) + gz_k, s_{vs} = c_p T_s(1 + \varepsilon q_s) + gz_s, and\ \varepsilon = \frac{R_{vap}}{R_{dry}} - 1,$$

where z is the height, g is the acceleration of gravity, S_v is the virtual dry static energy, U and V are zonal and meridional wind components, c_p is the specific heat at constant pressure of moist air, T is temperature, ε is parcel entrainment (R_{vap} and R_{dry} is gas constant for water vapor and for dry air respectively), q is specific humidity and the subscript k and s represent the level and the surface (lowest level) respectively. Here we set g as 9.8 m/s^2, U_s and V_s as zero, c_p as 1004.7 J/kg, ε as 0.61.

ERA5 is newest global reanalysis produced by ECMWF (Biavati et al., 2020). ERA5 has hourly output throughout, 31 km horizontal resolution, and 137 vertical levels from the surface up to a height of 80km. ERA5 hourly PBLH, 2 m temperature, 100 m U & V, and sea surface pressure are used in this paper.

Ri for radiosondes is calculated using the same method as in ERA5 (ECMWF. IFS CY41R2 Part IV, https://www.ecmwf.int/node/16648). To assist in the calculation, the ERA5 data were linearly interpolated to the locations of radiosonde data. To compare the wind components, U & V in radiosonde data were linearly interpolated to 100 m height.

3 Results

The observed PBLH of each cruise, as well as the lowest temperature, were shown in Figure 2, and the mean values and other parameters of observed and ERA5 PBLH were listed in Table 1. As shown in Table 1, the mean of observed PBLH was 488.0 m, and the standard deviation (STD) was 253.6 m. The mean of ERA5 PBLH after interpolation was 485.2 m, and the STD was 226.1 m. However, the root-mean-square error (RMSE) between ERA5 and observed PBLH was 201.3 m averaged over all the cruises and varied from 143.4 m for cruise Mirai2014 to 345.4 m for cruise Louis2014 (Table 1), indicating some large differences at individual location.

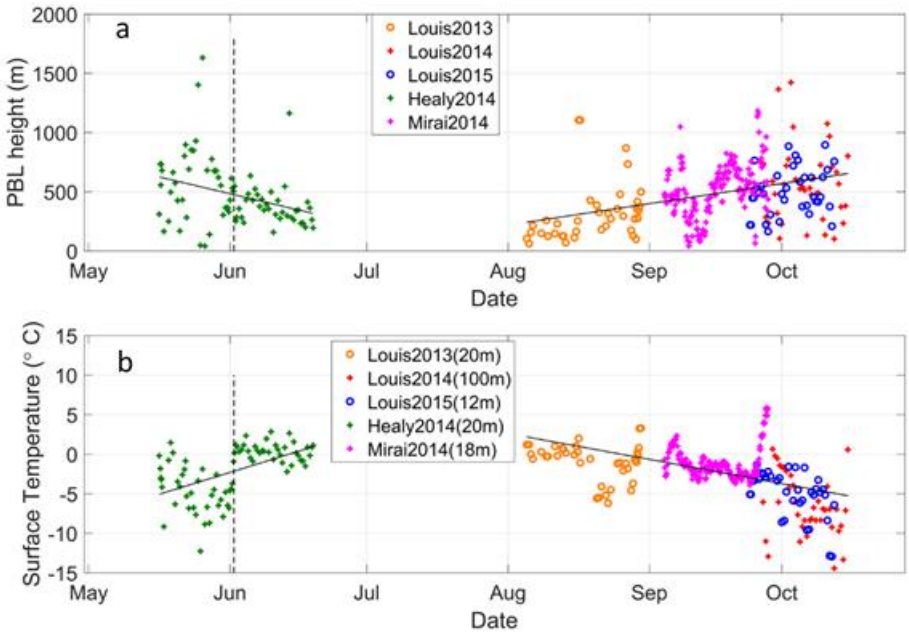

Figure 2. Planetary boundary layer heights (**a**) and the lowest level temperature (**b**) obtained from the radiosonde data of the cruises. The straight lines are the least squares fits for early summer and early autumn. The lowest level heights are labeled correspondingly. The vertical dashed lines divided Healy2014 into a cold and warm period.

Table1. Mean PBLH (m) from ERA5 and each cruise

Period	ERA5 mean (STD)	Observation mean (STD)	Correlation coefficient	RMSE	Bias Error
Total	485.2 (226.1)	488.0 (253.6)	0.63	206.9	-2.8
Louis2013	247.9 (160.2)	315.7 (248.4)	0.36	251.2	-67.8
Louis2014	352.7 (190.6)	562.1 (312.5)	0.49	345.4	-209.4
Louis2015	499.1 (226.4)	501.3 (194.8)	0.73	157.0	-2.2
Mirai2014	577.0 (196.6)	511.8 (223.8)	0.82	143.4	65.2
Healy2014	445.7 (205.0)	475.7 (276.5)	0.55	237.8	-30.1
Healy2014(cold)	519.8 (237.4)	568.8 (321.7)	0.50	292.2	-49.0
Healy2014(warm)	367.5 (122.6)	377.7 (170.8)	0.43	161.8	-10.1

The seasonal variations in PBLH were evident for the observational results (Figure 2a), and for the ERA5 results (Figure S1a). In the period of the observations, PBLH decreased from mid-May (~ 570 m) to mid-June (~ 280 m) and increased after August (~ 150 m) to October (~ 570 m), which is opposite to the variation of air temperature at the lowest levels (defined as surface air temperature in this study) (Figure 2b & Figure S1b). This seasonal variation of PBLH is roughly consistent with the previous study using the aircraft and GPS soundings in SHEBA (Dai et al., 2011). The storm events were found more numerous (Sorteberg & Walsh, 2008) and more intense (X. Zhang et al., 2004) in winter than in summer over Chukchi-Beaufort Sea, which might contribute to the observed and modeled seasonal variability in PBLH.

To elucidate the impact of surface air temperatures on the PBLH, we consider the case of the Healy2014 cruise during which there was a marked transition from cold (~ -4°C) to warm (~ 0.4°C) conditions (Fig S2). This transition occurred on June 2nd, 2014, and we used this date to divide the cruise period into a cold and warm period. For the entire Healy period, the average observed PLBH was 475.7 m, and the RMSE between ERA5 and observed PBLH was 237.8 m. The mean PBLH for the cold period (568.8 ±321.7 m) was much larger than that for the warm period (377.7±170.8 m). The ERA5 PBLH were slightly lower than the observation but also show this clear shift (519.8±321.7 m for the cold period and 367.5±122.6 m for the warm period). The bias error of ERA5 in cold period was -49.0 m and in warm period was -10.1 m, and the RMSEs between ERA5 and observation were 292.2 m and 161.8 m respectively. With comparison among these results in Table 1, except Mirai2014, it can be concluded that the higher PBLH are, the higher variances and the higher simulated errors will be.

To understand the synoptic conditions that gave rise to this transition, we considered the surface flow as represented in ERA5 over the region of interest during the cold and warm periods (Figure S3). During the cold period, corresponding to the high PBLH and the large bias between the observations and ERA5, the Healy was situated to the east of a region of high pressure, with

186 northerly winds being dominant. In contrast, during the warm period, corresponding to low
187 PBLH and the small bias, the Healy was situated to the west of a region of high pressure, with
188 southerly winds being dominant.

189 The Healy observations suggest that there may be a relationship between the bias error in
190 PBL and the direction of the meridional wind as well as surface temperature. To test this
191 hypothesis, we used the entire database and stratified the results by wind component and
192 temperature (Figure 3). We used ERA5 winds at 100 m height, in order to be consistent with the
193 following comparisons, because the heights of lowest level in different cruises are different and
194 ERA5 provides the product of winds at 100 m. We picked the calendar time of composite
195 analysis by the PBLH differences between ERA5 and observations whether positive greater than
196 1 STD or negative greater than -1 STD. The results are subtracted out the long mean for the
197 period of interest (1979 to 2018) to avoid the seasonal and diurnal differences.

198

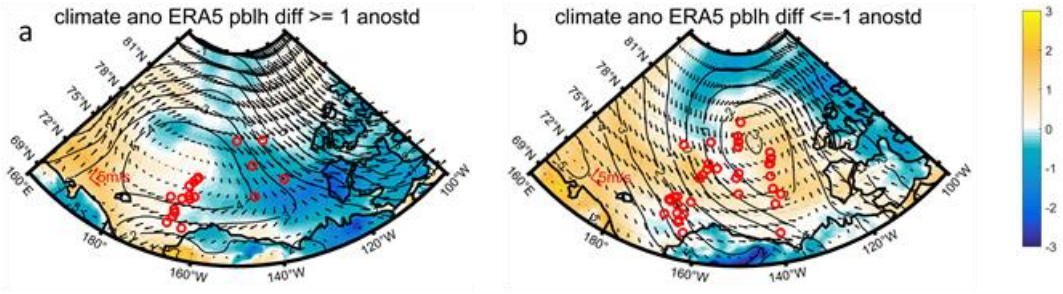

199

200 **Figure 3**. Anomalies of temperature (shading), sea level pressure (contours), and winds (arrows)
201 for the times when ERA5 planetary boundary layer heights had the positive biases that was
202 greater than +1 STD (**a**) and the times when the negative bias was greater than -1 STD (**b**). The
203 locations of the icebreaker observations with such large biases are marked by red circles.

204

205 Consistent with the hypothesis noted above, the large biases mainly occurred when the
206 northerly winds were dominant, independent of whether the bias was positive (Figure 3a) or
207 negative (Figure 3b). ERA5 more likely holds large positive bias of PBLH at the east of the high-
208 pressure anomalies when the high-pressure anomalies are over the Chukchi Sea. And ERA5
209 more likely hold large negative biases of PBLH at the southwest of the low-pressure anomalies
210 when the low-pressure anomalies are over the Beaufort Sea.

211 For further verification of the relationship between the PBLH biases and the northerly
212 winds, we show the dotted points with plus symbol by each variation and the PBLH differences
213 between ERA5 and observation as coordinates (Figure 4). We divided the whole 373
214 observations into six boxes with two black ±1 STD lines and one zero line (mean value line for
215 PBLH). We cycle large biases of each variation to avoid ERA5 biases in other variations
216 influencing our estimate. According to Figure 4a&b, ERA5 hold huge negative biases when the
217 observed PBLH are large, and huge positive biases when the observed PBLH are small. It is
218 worth noting that the air temperatures biases could cause PBLH biases, when ERA5 simulate air
219 temperature lower than observation, the PBLH in ERA5 is generally lower than the observed
220 PBLH, and vice versa (Figure 4c&d). The zonal winds have no obvious and consistent influence
221 according to Figure 4e&f. The number counts in Figure 4g&h show the preponderant and

consistent results that more cases of large biases occur under the influences of northerly winds whether the bias is positive or negative, although the huge biases occur both sides of V winds.

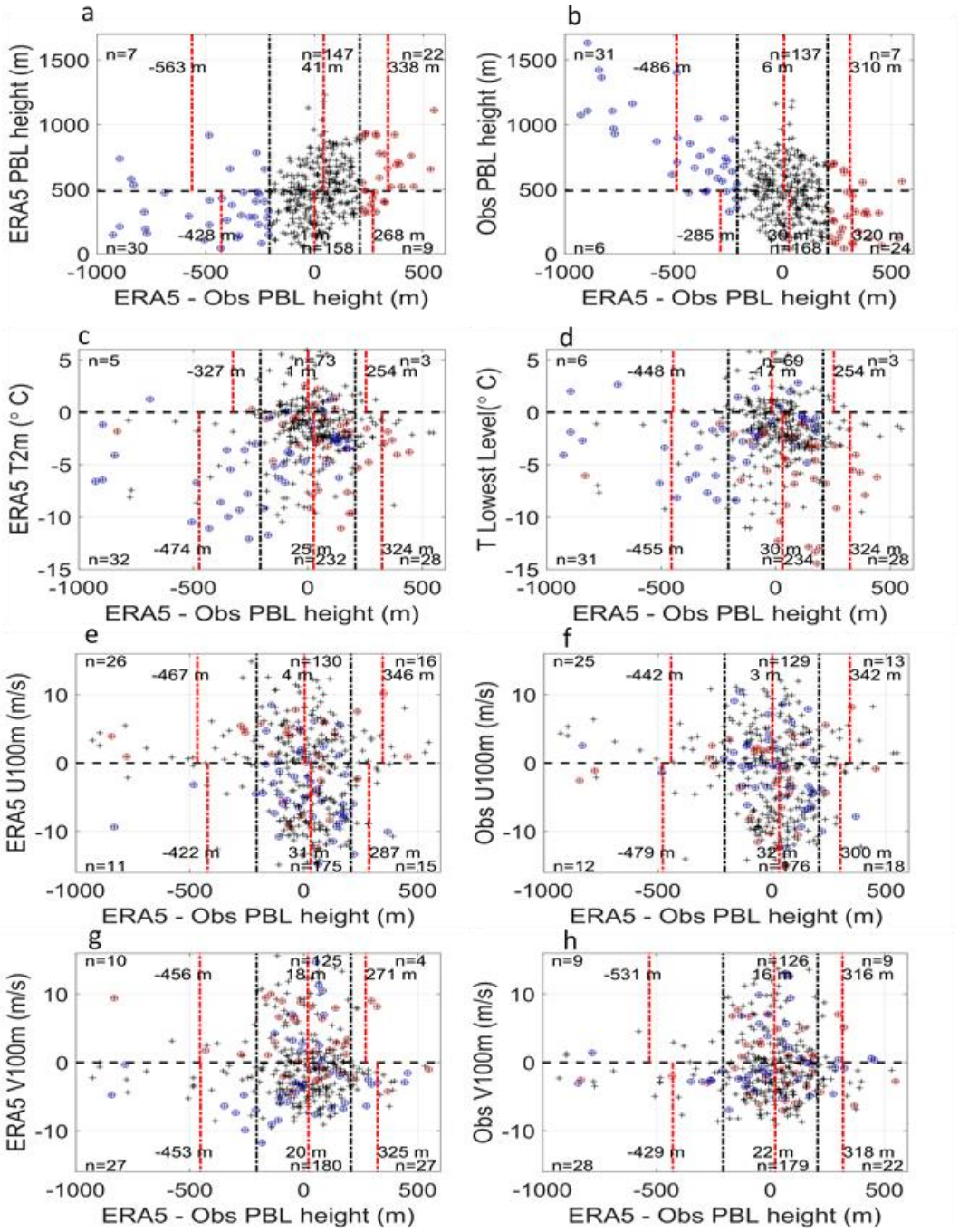

Figure 4. Relationship between ERA5 PBLH bias and ERA5 PBLH (**a**), observed PBLH (**b**), ERA5 T2m (**c**), observed lowest level temperature (**d**), ERA5 U100m (**e**), observed U100m (**f**), ERA5 V100m (**g**) and observed V100m (**h**). The black dashed line in (**a**) and (**b**) is the mean of ERA5 PBLH, while in the other sub-figures is zero. The black dash-dotted lines are ±1 STD of ERA5 PBLH biases. These black lines divided the whole observations into six boxes. The red

dash-dotted line is the mean PBLH anomaly of each box. The count value and the mean anomaly value are shown in each box. The blue cycles show the points with large negative biases of the variable used in the ordinate, while the red cycles show the points with large positive biases.

4 Conclusions and Discussions

We analyzed PBLH of five cruises observed at 2013~2015 late spring to autumn in the Chukchi-Beaufort Sea, and compared them with ERA5 results. It turns out that PBLH hold clear seasonal changes. The mean and STD of PBLH decreased from late autumn to the summer and then increased back when it comes to autumn. Esau & Sorokina (2011) mentioned some aspects of the seasonal cycle of PBLH. They mainly focus on the climatology of Arctic PBL and divided the whole Arctic into several regions but did not separate the ice edge zone individually. For the "central Arctic" region which included the Chukchi-Beaufort Sea in their work, the PBLH is greatest during summer months, same with the seasonal cycle in continental regions, because the domination of sea ice makes it more like continental. For the other maritime regions, the PBLH is greatest during winter and spring months when the air-sea temperature difference is greatest. Our results indicate that the seasonal change of PBLH at the ice edge zone is more like the marine zone instead of the continental zone.

Consistent with previous studies (Chan & Wood, 2013; Davy et al., 2017; Guo et al., 2016), surface temperature has an significant influence on the magnitude and the variance of PBLH. Surface temperature also has a significant effect on ERA5 PBLH simulation performance. When ERA5 simulate air temperature lower than observation, it is highly possible simulate PBLH lower than observation, and vice versa.

The Arctic has a limited number of in-situ observations and as well, it is a region where it remains a challenge to assimilate satellite observations into numerical weather prediction models (Lawrence et al., 2019). It follows that the observed bias when stratified by wind direction may also be attributed to the fact southerly flow advects information from land-based stations into the region thereby improving the representation of the PBLH in ERA5 (Ghil et al., 1981; Jung et al., 2016). This characteristic may contribute to our finding that large biases of the ERA5 PBLH are more common when there are northerly winds.

Acknowledgments and Data Resources

This study was supported by the National Key R&D Program of China (2016YFA0601804) and by the National Natural Science Foundation of China (Grant Nos. 41941007 and 41876220). MG was supported by the program of China Scholarships Council (No.201908320511). We thank the Office of Naval Research (ONR) for funding the cruises Healy2014, Louis2013, Louis2014 and Louis2015. We thank all scientists and staff members who are contribute to the observation and reanalysis data achieve. The data of Healy2014, Louis2013, Louis2014 and Louis2015 could be found at https://doi.org/10.5683/SP2/1OIWSO. The data of Mirai2014 could be downloaded at Japan Agency for Marine-Earth Science and Technology (2016) Data and Sample Research System for Whole Cruise Information in JAMSTEC (DARWIN): http://www.godac.jamstec.go.jp/cruisedata/mirai/e/index.html. ERA5 data are available at https://www.ecmwf.int/en/forecasts/datasets/reanalysis-datasets/era5.

References

Bian, L., Ding, M., Lin, X., Lu, C., & Gao, Z. (2016). Structure of summer atmospheric boundary layer in the center of Arctic Ocean and its relation with sea ice extent change. *Science China Earth Sciences*, *59*(5), 1057–1065.

Biavati, G., Bidlot, J., Bonavita, M., Chiara, G. De, Dahlgren, P., Dee, D., Diamantakis, M., Dragani, R., Flemming, J., Forbes, R., Fuentes, M., Geer, A., Haimberger, L., Healy, S., & Hogan, R. J. (2020). The ERA5 Global Reanalysis. *Quarterly Journal of the Royal Meteorological Society*. https://doi.org/10.1002/qj.3803

Bintanja, R., Graversen, R. G., & Hazeleger, W. (2011). Arctic winter warming amplified by the thermal inversion and consequent low infrared cooling to space. *Nature Geoscience*, *4*(11), 758–761. https://doi.org/10.1038/ngeo1285

Brooks, I. M., Tjernström, M., Persson, P. O. G., Shupe, M. D., Atkinson, R. A., Canut, G., Birch, C. E., Mauritsen, T., Sedlar, J., & Brooks, B. J. (2017). The turbulent structure of the Arctic summer boundary layer during the Arctic Summer Cloud-Ocean Study. *Journal of Geophysical Research: Atmospheres*, *122*(18), 9685–9704.

Chan, K. M., & Wood, R. (2013). The seasonal cycle of planetary boundary layer depth determined using COSMIC radio occultation data. *Journal of Geophysical Research Atmospheres*, *118*(22), 12,422-12,434. https://doi.org/10.1002/2013JD020147

Dai, C.-Y., Gao, Z.-Q., Wang, Q., & Cheng, G. (2011). Analysis of Atmospheric Boundary Layer Height Characteristics over the Arctic Ocean Using the Aircraft and GPS Soundings. In *Atmospheric and Oceanic Science Letters* (Vol. 4, Issue 2, pp. 124–130). https://doi.org/10.1080/16742834.2011.11446916

Davy, R., Esau, I., Chernokulsky, A., Outten, S., & Zilitinkevich, S. (2017). Diurnal asymmetry to the observed global warming. *International Journal of Climatology*, *37*(1), 79–93. https://doi.org/10.1002/joc.4688

Davy, R., & Ezau, I. (2014). *Planetary boundary layer depth in Global climate models induced biases in surface climatology*. *October*. http://arxiv.org/abs/1409.8426

Esau, I., Davy, R., & Outten, S. (2012). Complementary explanation of temperature response in the lower atmosphere. *Environmental Research Letters*, *7*(4). https://doi.org/10.1088/1748-9326/7/4/044026

Esau, I., & Sorokina, S. (2011). Climatology of the arctic planetary boundary layer. In *Atmospheric Turbulence, Meteorological Modeling and Aerodynamics* (pp. 3–58).

Esau, I., & Zilitinkevich, S. (2010). On the role of the planetary boundary layer depth in the climate system. *Advances in Science and Research*, *4*, 63–69. https://doi.org/10.5194/asr-4-63-2010

Ghatak, D., & Miller, J. (2013). Implications for Arctic amplification of changes in the strength of the water vapor feedback. *Journal of Geophysical Research Atmospheres*, *118*(14), 7569–7578. https://doi.org/10.1002/jgrd.50578

Ghil, M., Cohn, S., Tavantzis, J., Bube, K., & Isaacson, E. (1981). Applications of estimation

theory to numerical weather prediction. In *Modeling and simulation facility: research review, 1980-1981, (US NASA Goddard Space Flight Center, Greenbelt, MD; NASA-TM-83907)*. https://doi.org/10.1007/978-1-4612-5970-1_5

Grachev, A. A., Fairall, C. W., Persson, P. O. G., Andreas, E. L., & Guest, P. S. (2005). Stable boundary-layer scaling regimes: The SHEBA data. *Boundary-Layer Meteorology*, *116*(2), 201–235. https://doi.org/10.1007/s10546-004-2729-0

Graversen, R. G., Mauritsen, T., Tjernström, M., Källén, E., & Svensson, G. (2008). Vertical structure of recent Arctic warming. *Nature*, *451*(7174), 53–56. https://doi.org/10.1038/nature06502

Guo, J., Miao, Y., Zhang, Y., Liu, H., Li, Z., Zhang, W., He, J., Lou, M., Yan, Y., Bian, L., & Zhai, P. (2016). The climatology of planetary boundary layer height in China derived from radiosonde and reanalysis data. *Atmospheric Chemistry and Physics*, *16*(20), 13309–13319. https://doi.org/10.5194/acp-16-13309-2016

Hines, K. M., & Bromwich, D. H. (2017). Simulation of late summer arctic clouds during ASCOS with polar WRF. In *Monthly Weather Review* (Vol. 145, Issue 2, pp. 521–541). https://doi.org/10.1175/MWR-D-16-0079.1

Holtslag, A. A. M., Svensson, G., Baas, P., Basu, S., Beare, B., Beljaars, A. C. M., Bosveld, F. C., Cuxart, J., Lindvall, J., Steeneveld, G. J., Tjernström, M., & Van De Wiel, B. J. H. (2013). Stable atmospheric boundary layers and diurnal cycles: Challenges for weather and climate models. *Bulletin of the American Meteorological Society*, *94*(11), 1691–1706. https://doi.org/10.1175/BAMS-D-11-00187.1

Inoue, J., & Hori, M. E. (2011). Arctic cyclogenesis at the marginal ice zone: A contributory mechanism for the temperature amplification? *Geophysical Research Letters*, *38*(12).

Johannessen, O. M., Bengtsson, L., Miles, M. W., Kuzmina, S. I., Semenov, V. A., Alekseev, G. V., Nagurnyi, A. P., Zakharov, V. F., Bobylev, L. P., Pettersson, L. H., Hasselmann, K., & Cattle, H. P. (2004). Arctic climate change: observed and modelled temperature and sea-ice variability. *Tellus A: Dynamic Meteorology and Oceanography*, *56*(4), 328–341. https://doi.org/10.3402/tellusa.v56i4.14418

Jung, T., Gordon, N. D., Bauer, P., Bromwich, D. H., Chevallier, M., Day, J. J., Dawson, J., Doblas-Reyes, F., Fairall, C., Goessling, H. F., Holland, M., Inoue, J., Iversen, T., Klebe, S., Lemke, P., Losch, M., Makshtas, A., Mills, B., Nurmi, P., … Yang, Q. (2016). Advancing polar prediction capabilities on daily to seasonal time scales. *Bulletin of the American Meteorological Society*, *97*(9), 1631–1647. https://doi.org/10.1175/BAMS-D-14-00246.1

Lai, H. W., Zhang, F., Clothiaux, E. E., Stauffer, D. R., Gaudet, B. J., Verlinde, J., & Chen, D. (2020). Modeling Arctic Boundary Layer Cloud Streets at Grey-zone Resolutions. *Advances in Atmospheric Sciences*, *37*(1), 42–56. https://doi.org/10.1007/s00376-019-9105-y

Lawrence, H., Bormann, N., Sandu, I., Day, J., Farnan, J., & Bauer, P. (2019). Use and impact of Arctic observations in the ECMWF Numerical Weather Prediction system. *Quarterly Journal of the Royal Meteorological Society*, *145*(725), 3432–3454. https://doi.org/10.1002/qj.3628

Li, X., Krueger, S. K., Strong, C., Mace, G. G., & Benson, S. (2020). Midwinter Arctic leads form and dissipate low clouds. *Nature Communications*, *11*(1), 1–8.

Liu, S., & Liang, X. Z. (2010). Observed diurnal cycle climatology of planetary boundary layer height. *Journal of Climate*, *23*(21), 5790–5809. https://doi.org/10.1175/2010JCLI3552.1

Persson, P. O. G., Fairall, C. W., Andreas, E. L., Guest, P. S., & Perovich, D. K. (2002). Measurements near the Atmospheric Surface Flux Group tower at SHEBA: Near-surface conditions and surface energy budget. *Journal of Geophysical Research: Oceans*, *107*(C10), SHE-21.

Pithan, F., & Mauritsen, T. (2014). Arctic amplification dominated by temperature feedbacks in contemporary climate models. *Nature Geoscience*, *7*(3), 181–184.

Romanov, I. P., Konstantinov, Y. B., & Kornilov, N. A. (2000). North Pole Drifting Stations (1937 [–] 1991). *Arctic Climatology Project, Environmental Working Group. Arctic Meteorology and Climate Atlas*.

Sato, K., Inoue, J., Kodama, Y., & Overland, J. E. (2012). Impact of Arctic sea-ice retreat on the recent change in cloud-base height during autumn. *Geophysical Research Letters*, *39*(10).

Screen, J. A. (2014). Arctic amplification decreases temperature variance in northern mid- to high-latitudes. In *Nature Climate Change* (Vol. 4, Issue 7, pp. 577–582). https://doi.org/10.1038/nclimate2268

Screen, J. A., & Simmonds, I. (2010). The central role of diminishing sea ice in recent Arctic temperature amplification. *Nature*, *464*(7293), 1334–1337.

Seidel, D. J., Zhang, Y., Beljaars, A., Golaz, J. C., Jacobson, A. R., & Medeiros, B. (2012). Climatology of the planetary boundary layer over the continental United States and Europe. *Journal of Geophysical Research Atmospheres*, *117*(17), 1–15. https://doi.org/10.1029/2012JD018143

Seo, H., & Yang, J. (2013). Dynamical response of the Arctic atmospheric boundary layer process to uncertainties in sea-ice concentration. *Journal of Geophysical Research Atmospheres*, *118*(22), 12,383-12,402. https://doi.org/10.1002/2013JD020312

Serreze, M. C., Barrett, A. P., Stroeve, J. C., Kindig, D. N., & Holland, M. M. (2009). The emergence of surface-based Arctic amplification. In *Cryosphere* (Vol. 3, Issue 1, pp. 11–19). https://doi.org/10.5194/tc-3-11-2009

Serreze, M. C., & Barry, R. G. (2011). Processes and impacts of Arctic amplification: A research synthesis. In *Global and Planetary Change* (Vol. 77, Issues 1–2, pp. 85–96). https://doi.org/10.1016/j.gloplacha.2011.03.004

Serreze, M. C., & Francis, J. A. (2006). The arctic amplification debate. In *Climatic Change* (Vol. 76, Issues 3–4, pp. 241–264). https://doi.org/10.1007/s10584-005-9017-y

Shupe, M. D., Persson, P. O. G., Brooks, I. M., Tjernström, M., Sedlar, J., Mauritsen, T., Sjogren, S., & Leck, C. (2013). Cloud and boundary layer interactions over the Arctic sea ice in late summer. In *Atmospheric Chemistry and Physics* (Vol. 13, Issue 18, pp. 9379–9400). https://doi.org/10.5194/acp-13-9379-2013

Sorteberg, A., & Walsh, J. E. (2008). Seasonal cyclone variability at 70°N and its impact on moisture transport into the Arctic. *Tellus, Series A: Dynamic Meteorology and Oceanography*, *60 A*(3), 570–586. https://doi.org/10.1111/j.1600-0870.2008.00314.x

Tjernström, M., & Graversen, R. G. (2009). The vertical structure of the lower Arctic troposphere analysed from observations and the ERA-40 reanalysis. *Quarterly Journal of the Royal Meteorological Society: A Journal of the Atmospheric Sciences, Applied Meteorology and Physical Oceanography*, *135*(639), 431–443.

Wood, R. (2012). Stratocumulus clouds. *Monthly Weather Review*, *140*(8), 2373–2423. https://doi.org/10.1175/MWR-D-11-00121.1

Yang, X. Y., Fyfe, J. C., & Flato, G. M. (2010). The role of poleward energy transport in arctic temperature evolution. *Geophysical Research Letters*, *37*(14), 1–5. https://doi.org/10.1029/2010GL043934

Zhang, X., Walsh, J. E., Zhang, J., Bhatt, U. S., & Ikeda, M. (2004). Climatology and interannual variability of Arctic cyclone activity: 1948–2002. *Journal of Climate*, *17*(12), 2300–2317.

Zhang, Y., Gao, Z., Li, D., Li, Y., Zhang, N., Zhao, X., & Chen, J. (2014). On the computation of planetary boundary-layer height using the bulk Richardson number method. *Geoscientific Model Development*, *7*(6), 2599–2611. https://doi.org/10.5194/gmd-7-2599-2014